ELSEVIER

Contents lists available at ScienceDirect

Archives of Biochemistry and Biophysics

journal homepage: www.elsevier.com/locate/yabbi





Mutational analysis confirms the presence of distal inhibitor-selectivity determining residues in *B. stearothermophilus* dihydrofolate reductase

Tyler Eck, Seema Patel, Thomas Candela, Katherine Leon H, Michael Little, Natalia E. Reis, Uththara Liyanagunawardana, Ueli Gubler, Cheryl A. Janson, Jaclyn Catalano, Nina M. Goodey *

Dept. of Chemistry & Biochemistry, Montclair State University, Montclair, NJ, 07043, USA

ARTICLE INFO

Keywords:
DHFR
Trimethoprim
Pyrimethamine
Distal residues
Drug binding
Inhibitor selectivity

ABSTRACT

Many antibacterial and antiparasitic drugs work by competitively inhibiting dihydrofolate reductase (DHFR), a vital enzyme in folate metabolism. The interactions between inhibitors and DHFR active site residues are known in many homologs but the contributions from distal residues are less understood. Identifying distal residues that aid in inhibitor binding can improve targeted drug development programs by accounting for distant influences that may be less conserved and subject to frequent resistance causing mutations. Previously, a novel, homologybased, computational approach that mines ligand inhibition data was used to predict residues involved in inhibitor selectivity in the DHFR family. Expectedly, some inhibitor selectivity determining residue positions were predicted to lie in the active site and coincide with experimentally known inhibitor selectivity determining positions. However, other residues that group spatially in clusters distal to the active site have not been previously investigated. In this study, the effect of introducing amino acid substitutions at one of these predicted clusters (His38-Ala39-Ile40) on the inhibitor selectivity profile in Bacillus stearothermophilus dihydrofolate reductase (Bs DHFR) was investigated. Mutations were introduced into these cluster positions to change sidechain chemistry and size. We determined $k_{\rm cat}$ and $K_{\rm M}$ values and measured $K_{\rm D}$ values at equilibrium for two competitive DHFR inhibitors, trimethoprim (TMP) and pyrimethamine (PYR). Mutations in the His38-Ala39-Ile40 cluster significantly impacted inhibitor binding and TMP/PYR selectivity - seven out of nine mutations resulted in tighter binding to PYR when compared to TMP. These data suggest that the His38-Ala39-Ile40 cluster is a distal inhibitor selectivity determining region that favors PYR binding in Bs DHFR and, possibly, throughout the DHFR family.

1. Introduction

Dihydrofolate reductase (DHFR) catalyzes the NADPH dependent reduction of dihydrofolate (DHF) into tetrahydrofolate (THF), a precursor in the synthesis of DNA bases [1]. As such, DHFR is the target of inhibitors used to treat bacterial and parasitic infections as well as cancer. Well-known competitive DHFR inhibitors include methotrexate (MTX), trimethoprim (TMP), and pyrimethamine (PYR) [2–5]. Their potencies vary across the DHFR family; for example, TMP inhibits *Escherichia coli (Ec)* DHFR at lower concentrations than human (*Hs*) DHFR [6,7]. In this manuscript, we refer to the selective binding of multiple inhibitors to a single DHFR enzyme as the enzyme's "inhibitor selectivity profile".

DHFR mutagenesis has revealed key amino acid residues involved in inhibitor binding, catalysis, and conformational motions [2,8–13]. Most

of the inhibitor binding determinants that have been investigated are located in the active site. However, similar to what has been found for other enzymes such as HIV protease [14], it is likely that residues outside of the DHFR active site (distal residues) also influence inhibitor binding [15]. A better understanding of how such distal residues affect enzyme function and inhibitor binding can improve rational protein engineering and drug discovery programs. Therefore, we set out to determine whether distal mutations in DHFR have similar or different effects on the binding of two known competitive DHFR inhibitors, TMP and PYR. Previous work has predicted that three amino acid residue positions (Asn48, Leu49, and Val50, Hs DHFR numbering) in the DHFR family play a role in determining inhibitor selectivity [16]. These residues are located in the BC-strand, which is distal to the active site, suggesting that they may act by perturbing amino acid networks [17]. These distal effects can influence an enzyme's binding properties by perturbing an enzyme's conformational equilibrium [17-20]. Enzymes

E-mail address: goodeyn@mail.montclair.edu (N.M. Goodey).

^{*} Corresponding author.

Abbreviations

DHFR Dihydrofolate reductase

NADPH Dihydronicotinamide-adenine dinucleotide phosphate

DHF Dihydrofolate
THF Tetrahydrofolate
TMP Trimethoprim
PYR Pyrimethamine
MTX Methotrexate

IPTG Isopropyl-β-D-thiogalactoside

Bs DHFR Bacillus stearothermophilus DHFR

MTS 3-(4,5-dimethylthiazol-2-yl)-5-(3-

carboxymethoxyphenyl)-2-(4-sulfophenyl)-2H-

tetrazolium

Mt DHFR Mycobacterium tuberculosis DHFR

Ec DHFR Escherichia coli DHFR Hs DHFR human DHFR

have multiple conformational sub-states that bind inhibitors with varying affinities, thus the inhibitor selectivity profile can be affected when a mutation perturbs the sampling of enzyme sub-states [21].

We used the moderate thermophile *Bacillus stearothermophilus* DHFR (Bs DHFR) as a model system [22]. As an initial exploratory analysis following the *in silico* results, we generated a limited set of mutants in both the predicted cluster and the active site. The resulting proteins were expressed and purified and their k_{cat} and k_{M} values were determined. We adapted intrinsic protein fluorescence protocols to a microplate reader format to determine direct k_{D} values for thermostable wild type and mutant k_{D} DHFR proteins toward TMP and PYR, using the long incubation times necessary to reach equilibrium [23].

2. Materials and methods

2.1. Randomized mutagenesis of the Bs DHFR gene

Site-directed and randomized mutageneses were performed on the Bs DHFR gene cloned into the pET21a + expression vector (a kind gift from Judith Klinman) using PCR [22]. Mutagenic primers were created with a 3'overhang, incorporating the desired mutation at least five bases from the 5' end [24]. Integrated DNA Technologies, Inc. provided the oligonucleotides for mutagenesis; the sequences can be found in Supplemental Table S1. Each mutagenesis reaction consisted of 0.5 μM of the forward and reverse mutagenic primers, 50-70 ng DNA template, 0.2 mM dNTPs, 0.5 uL (1 U) Phusion DNA polymerase (Thermo Fisher Scientific, Cat #F530S), and 1X HF-buffer (Thermo Fisher Scientific, Cat #F530S) in a total volume of 50 μL. The PCR reaction was performed using the following parameters. Initial denaturation was conducted at 98 °C for 5 min, followed by 35 cycles of 98 °C for 30 s, and 72 °C for 6 min, with a final extension at 72 °C for 10 min. After completion of the PCR protocol, 10 units of DpnI (Fisher Scientific, Cat # FERER1701) were added to each reaction followed by an incubation at 37 °C for 1 h. XL Blue cells were transformed with 1 µL of the digested product using the protocol described below. DNA plasmids of successful transformants were isolated and sequenced at the Biology Department of Montclair State University.

2.2. Chemical transformation of XL1 blue and BL21 strains

Using chemically competent cells, 1–5 μL of wild type or mutated pET21a + DHFR plasmid were added to 50 μL of the competent cells. The cells were incubated on ice for 30 min then placed into a 42 °C water bath for 45 s. The cells were placed on ice for 2 min before adding 0.9 mL of sterile LB broth preheated to 37 °C. The cells were allowed to recover

for 1 h at 37 $^{\circ}$ C with shaking at 225 RPM. The mixture (100 μ L) was spread on sterile LB agar plates with 100 μ g/mL of ampicillin and incubated overnight at 37 $^{\circ}$ C. Colonies were then picked and suspended in 5 mL of LB, containing 100 μ g/mL of ampicillin, and grown overnight at 37 $^{\circ}$ C and 225 RPM. Plasmid DNA was purified using a QIAGEN MiniPrep kit.

2.3. Expression and purification of Bs DHFR proteins

Cloned wild-type and mutant Bs DHFR genes were expressed in BL21 cells under the control of the inducible T7 promotor [22]. Starter cultures for each protein to be expressed included 5 mL LB with $100 \,\mu g/mL$ ampicillin and were grown to saturation overnight at 37 °C while shaking at 225 RPM. The following day, fresh LB (125-500 mL) was inoculated with 1/100th volume of the saturated overnight culture volume and grown to an OD600 of 0.6-0.8 at 37 °C and 225 RPM. Expression was induced with 1.0 mM IPTG, followed by an overnight incubation at 30 °C and 225 RPM. Cells were pelleted and resuspended in B-Per Protein Extraction Solution (Thermo Fisher Scientific, Cat # 78243), at a ratio of 4 mL reagent for every 1 g of wet cell pellet, and incubated at room temperature for 15 min. The cell lysate was centrifuged at 15.000×g for 20 min. Protein purification from the soluble supernatant fraction was done in one step with an SP Sepharose Fast Flow cation exchange column (Fisher Scientific, Cat # 45-002-934), using 40 mM HEPES buffer, 1 mM DTT at pH 6.8 to bind and wash and 40 mM HEPES, 1 mM DTT, and 0.2 M NaCl to elute the protein from the column [22]. Enzyme concentrations were spectroscopically determined at 280 nm using the molar extinction coefficient 25,565 M⁻¹cm⁻¹ [21]. Protein purity was determined by SDS-PAGE analysis.

2.4. Circular dichroism spectroscopy

Bs DHFR mutant proteins were buffer exchanged into 50 mM potassium phosphate at pH 7.4 to remove the high chloride concentration in the elution buffer. Samples were reduced using a PierceTM Immobilized TCEP Disulfide Reducing Gel (Thermo Scientific), while vortexing for 20 min. Upon centrifugation, the reduced Bs DHFR mutants were diluted to 4.6–6.2 μM in 400 μL of 50 mM potassium phosphate at pH 7.4. Circular dichroism (CD) spectra were collected using an Applied Photophysics Chirascan with the following parameters: the bandwidth was 0.5 nm, the wavelength range was 190 nm-280 nm with a step of 0.5 nm, time-per-point was 0.5 s, the baseline was automatically subtracted, and adaptive sampling was enabled. Each sample was scanned five times and the traces were smoothed with a window scale of five and averaged. The 50 mM potassium phosphate buffer at pH 7.4 was used for the baseline and for each scan. The CD signals were converted from mdeg to molar ellipticity to take into consideration small differences in enzyme concentrations.

2.5. Determination of k_{cat} and K_M values

Bs DHFR turnover numbers (k_{cat}) were obtained by tracking the disappearance of DHF and NADPH cofactor through a decrease in absorbance at 340 nm in a microtiter plate-based assay (200 μL) using a Synergy H1 platereader [25]. Saturating concentrations of DHF and NADPH (100 μM) were used in HEPES buffer (40 mM HEPES, 1 mM DTT, pH 6.8) and the reaction was initiated by adding enzyme to 0.05–2.05 μM. The slopes of the graphs (absorbance at 340 nm/s) were converted to velocities (mM/s) using the molar extinction coefficient for the equimolar mix of DHF and NADPH, 13.2 (mM $^{-1}$ cm $^{-1}$) and a 0.46 cm pathlength [25]. The pathlength was determined using the Synergy H1 pathlength determination software, which measures the absorbance of water at 900 nm and 977 nm in the 200 μL reaction mixture. The wild type enzyme was used as a positive control at 50 nM for every mutant enzyme experiment.

K_M values were determined as above except that enzyme and DHF

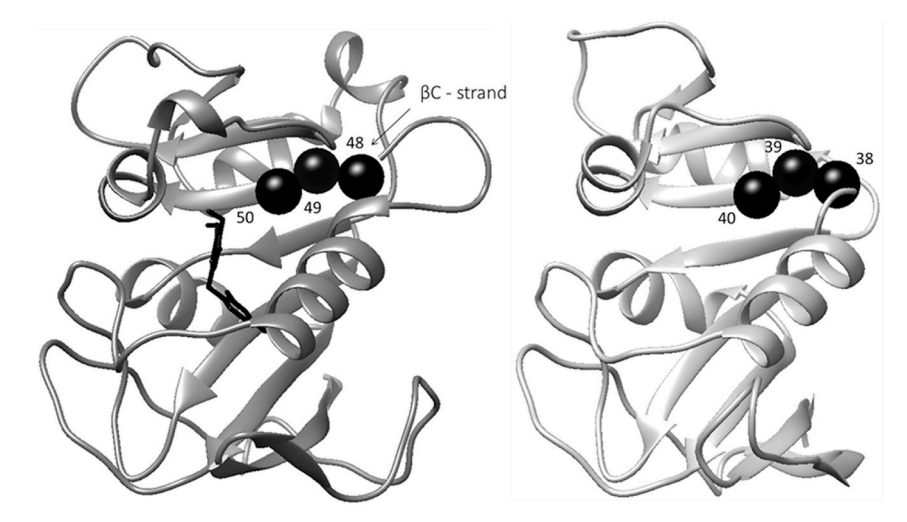


Fig. 1. Cartoon representation of the *Hs* DHFR (Left, PDB #: 2W3A) in dark grey lines and *Bs* DHFR (Right, PDB #: 1ZDR) in light grey lines [22]. The alpha carbons of the Asn48-Leu49-Val50 residues are represented in the *Hs* DHFR by black spheres, with equivalent residues (His38-Ala39-Ile40) in the *Bs* DHFR also shown as black spheres and numbered accordingly. This figure was made using the Match Maker tool of Chimera Software (version 1.11.2) [30].

concentrations ranged between 5 and 15 nM and 234 nM - 120 μM , respectively and the reaction was monitored using 3-(4,5-dimethylthiazol-2-yl)-5-(3-carboxymethoxyphenyl)-2-(4-sulfophenyl)-2H-tetrazolium (MTS) (Fisher Scientific, Cat # NC1508746). Following absorbance at 340 nm at DHF concentrations below 2 μM gave small signal changes and signal-to-noise ratios. Reduction of MTS by THF produces a formazan product that has a greater molar extinction coefficient at 450 nm than that of combined NADPH and DHF at 340 nm [26]. For each experiment, a negative control containing only enzyme, NADPH, and MTS was monitored and the resulting signal was subsequently subtracted from all other reaction values determined in the presence of DHF. The K_{M} was determined by plotting the velocities against DHF concentration and fitting to the Michaelis-Menten equation in Kaleida-Graph. Reported steady state values are the average of three replicate measurements unless specified otherwise.

2.6. Determining K_D by fluorescent equilibrium titration

Bs DHFR enzyme proteins (600 nM) were mixed with 100 μM NADPH and TMP or PYR at concentrations ranging from 22 nM to 2000 nM in 40 mM HEPES buffer pH 6.8 containing 1 mM DTT. Incubations were carried out at room temperature for 30 min to allow adequate time for equilibrium to be reached [27]. Data was collected using a Synergy H1 microplate reader in fluorescence mode using a Xenon flash light source from the top face of the microtiter plate. The temperature was set to 25 °C before taking measurements. The excitation wavelength was 290 nm, while the fluorescence emission was recorded at 340 nm; emission from NADPH due to fluorescence energy transfer was measured at 450 nm. The read height was 7 mm, and gain was 140 for 340 nm emission and 110 for the 450 nm emission. Fluorescence emission intensity at 340 nm or 450 nm was graphed against the corresponding inhibitor concentration using Microsoft Excel. Signal averaging of the fluorescence emission intensity was performed with three measurements that yielded an averaged graph, which constituted one trial. An inner filter correction was applied to account for any effect the titrating inhibitor may have had on the fluorescence signal [28]. The inner filter correction values were determined via the same protocol that was used to determine the K_D values except that Bs DHFR in the well was replaced with 150 nM of tryptophan. To obtain the inner filter correction values, the fluorescence intensity values at each concentration of inhibitor were measured and normalized to the fluorescence intensity obtained in the absence of inhibitor. Finally, all experimental fluorescence intensities were corrected by dividing them by their corresponding inner filter correction values. K_D values were calculated from the corrected fluorescence intensity vs. inhibitor concentration data using a modified Morrison equation where F_{min} : minimum fluorescence signal, F_{max} : maximum fluorescence signal, [E]: enzyme concentration, and [I]: inhibitor concentration (Equation (1)) [29]. The K_D values reported are the result of at least three independent trials.

$$F = (F_{max} - F_{min}) * \left(\frac{([E] + [I] + K_D) - \sqrt{([E] + [I] + K_D)^2 - 4[E][I]}}{2[E]} \right) + F_{min}$$
(1)

2.7. Statistical analyses

We used IBM SPSS Statistics 25 to perform Student's t tests. This was done, in some cases, to compare a specific K_D for one mutant to the wild type K_D , demonstrating the effects of the mutation on inhibitor binding. In other situations, we compared the K_D for TMP to K_D for PYR for a single mutant. This comparison showed whether there was a significant selectivity for one inhibitor over the other. Finally, we used Student's t tests to compare values for a position rather than a mutation. In these instances, we combined all values (for example K_D TMP) for one position (all replacements) and compared to all values for wild type. This allowed us to determine whether effects at a given position were solely due to the type of side chain used in the mutation, or if the overall location of the mutation was the key cause for the observed result.

3. Results

3.1. Steady-state kinetics of DHFR proteins with His38-Ala39-Ile40 cluster mutations

Previous work predicted that three amino acid residue positions (Asn48, Leu49, and Val50, *Hs* DHFR numbering) in the DHFR family play a role in determining inhibitor selectivity [16]. Here we investigated these residue positions experimentally in *Bs* DHFR. Since the *Bs* DHFR sequence was not part of the original *in silico* analysis, an alignment of the *Hs* and *Bs* DHFR structures was used to confirm that residue cluster Asn48-Leu49-Val50 in *Hs* DHFR is represented by positions His38-Ala39-Ile40 in *Bs* DHFR (Fig. 1).

Mutations at this cluster were generated using a pool of mutagenic primers that were randomized at these codon positions. The resulting mutants were screened for *in vivo* DHFR activity by determining their ability to support growth in a DHFR-deficient strain (Supplement;

Bacillus stearothermophilus	1	M	ISHIVAMDE-NRVIGKD-NRLPW-HLPADLAYFKRVTMG HAIVMGRKTFEAIGRPLPGRDNVVVTG	64
Bacillus subtilis	1	M	ISFIFAMDA-NRLIGKD-NDLPW-HLPNDLAYFKKITSG HSIMGRKTFESIGRPLPNRKNIVVTS	64
Shewanella oneidensis	1	M	RIAMIAAMAN-NRVIGKD-NKMPW-HLPEDLRHFKAMTLG KPVVMGRKTFESIGRPLPGRHNIVISR	65
Deinococcus radiodurans	1	M[1	2]RQDIVAIAAQTE-NRVIGRD-GGMPW-HLPADFAHFRALSVG KPNIMGRKVFDTLRRKPLPERVNIVLTR	80
Streptococcus pneumoniae	1	M	TKKIVAIWAQDE-EGLIGKE-NRLPW-HLPAELQHFKETTLN HAILMGRVTFDGMGRRLLPKRETLILTR	68
Pseudomonas aeruginosa	1	M	ARPLAMIAALGE-NRAIGID-NRLPW-RLPADLKHFKAMTLG KPVIMGRKTWDSLGRPLPGRLNLVVSR	67
Escherichia coli	1	M	ISLIAALAV-DRVIGME-NAMPW-NLPADLAWFKRNTLN KPVIMGRHTWESIGRPLPGRKNIILSS	64
Neisseria meningitidis	1	M	LK-ITLIAACAE-NLCIGAG-NAMPW-HIPEDFAFFKAYTLG KPVIMGRKTWESLPVKPLPGRRNIVISR	67
Mycobacterium tuberculosis	1	M	VGLIWAQAT-SGVIGRG-GDIPW-RLPEDQAHFREITMG HTIVMGRRTWDSLPAKVRPLPGRRNVVLSR	67
Drosophila melanogaster	1	M	LR-FNLIVAVCE-NFGIGIR-GDLPW-RIKSELKYFSRTTKR[7]NAVVMGRKTYFGVPESKRPLPDRLNIVLST	76
Mus musculus	1	M	VRPLNCIVAVSQ-NMGIGKN-GDLPWPPLRNEFKYFQRMTTT[7]NLVIMGRKTWFSIPEKNRPLKDRINIVLSR	78
Homo sapiens isoform 1	1	M	VGSLNCIVAVSQ-NMGIGKN-GDLPWPPLRNEFRYFQRMTTT[7]NLVIMGKKTWFSIPEKNRPLKGRINLVLSR	78
Caenorhabditis elegans	1	M	-RKMNLIVAMDA-EGGIGKN-GVLPW-RIKKDMQYFASVTKN[7]NAVLMGRKCWESIPVTRRPLAGRLNIVLSR	76
Dictyostelium discoideum	1	M	KVSIIVAVSK-NNVIGTKAGDIPW-ELPKDLKHFRDTTHG[1]-PCIIGRISLEAFGDLLPNRFNIIVSS	66
Saccharomyces cerevisiae	1] M	$5]$ PIVGIVACLQpEMGIGFR-G \overline{G} LPW-RLPS \overline{E} MKYFRQVTSL[7] \overline{NAL} IMGRKTWESIPPKFRPLPNRMNVIISR	81
Thermotoga maritima	1	-[3]VAKVIFVLAMDV-SGKIASSVESW-SSFEDRKNFRKITTE[2]-NVVMGRITFEEIGRPLPERLNVVLTR	69

Fig. 2. COBALT sequence alignment of select DHFR sequences from the Landmark Model Organisms database showing the region with the predicted His38-Ala39-Ile40 cluster positions. Bracketed numbers indicate amino acids not shown in the alignment sequence.

Table 1 Steady-state kinetic values of Bs DHFR mutants. All measurements were performed in triplicate and standard errors are shown. Values that are significantly different from the wild type value as determined by Student's t-test are indicated by asterisks as follows: *: p < 0.1, **: p < 0.05, ***: p < 0.01.

	$k_{\rm cat}$ (s ⁻¹)	K _M (μM)	k_{cat} (wild type)/ k_{cat} (mutant)	K_M (wild type)/ K_M (mutant)
Wild Type	8.1 ± 0.8	1.6 ± 0.4	-	-
His38Gln	10 ± 2	$\begin{array}{c} 1.6 \; \pm \\ 0.5 \end{array}$	0.8	1.0
His38Thr	5.4 ± 1.1	$\begin{array}{c} 0.98 \pm \\ 0.07 \end{array}$	1.5	1.6
His38Val	$5.5 \pm 0.4 \\ *$	$\begin{array}{c} 1.3 \pm \\ 0.2 \end{array}$	1.5	1.2
Ala39Ile	$\begin{array}{c} \textbf{4.0} \pm \textbf{0.7} \\ ** \end{array}$	1.5 ± 0.3	2.0	1.1
Ala39Arg	$^{4.6\pm1.0}_{*}$	$\begin{array}{c} 1.1 \; \pm \\ 0.3 \end{array}$	1.8	1.4
Ala39Tyr	6.7 ± 0.4	2.7 ± 1.0	1.2	0.6
Ile40Ala	6.6 ± 1.9	1.8 ± 1.1	1.2	0.9
Ile40Asn	5.0 ± 0.5	1.4 ± 0.5	1.6	1.1
Ile40Arg	$\begin{array}{c} 1.5 \pm 0.4 \\ *** \end{array}$	32. ± 13 *	5.4	0.05

Fig. S1). An alignment of DHFR protein sequences from the Landmark database showed varying degrees of conservation at residue positions equivalent to *Bs* DHFR residues 38–40 (Fig. 2 and Fig. S1) [31]. Position 38 showed a preference for polar or charged side chains, position 39 was occupied by a variety of residues with some tendency towards hydrophobic side chains, and position 40 was dominated by hydrophobic side chains.

For further analysis, we chose mutants that introduced side chains with different sizes and chemical characteristics compared to those found in the Bs DHFR wild type. We then expressed and purified the proteins, and determined their $k_{\rm cat}$ and $K_{\rm M}$ values. The largest change in $k_{\rm cat}$ was a five-fold reduction for the Ile40Arg mutant (Table 1). The other replacements (His38Gln, His38Thr, His38Val, Ala39Asn, Ala39Arg, Ala39Tyr, Ile40Ala, and Ile40Asn) resulted in only small changes in catalytic activity. Most of the mutant $K_{\rm M}$ values were similar to that of the wild type Bs DHFR as well. The Ile40Arg mutant was also the only mutant with a $K_{\rm M}$ that was significantly higher than the wild type $K_{\rm M}$ (t(2)=3.93, p=0.062). The Ile40Arg $k_{\rm cat}$ was measured using 100 μ M DHF, which may not be fully saturating given the high $K_{\rm M}$, and it is possible that the $k_{\rm cat}$ is higher than what is reported in Table 1.

Table 2

 $\rm K_D$ values for TMP and PYR for wild type $\it Bs$ DHFR and $\it Bs$ DHFR mutants are shown. Values are the average of three measurements unless otherwise noted in brackets; standard errors are reported. $\rm K_D$ values that are significantly different from the wild type values are indicated in the $\rm K_D$ columns by asterisks as follows: *: p < 0.1, **: p < 0.05, ***: p < 0.01. Asterisks in the Selectivity Score column indicate that $\rm K_D$ (TMP) is significantly different from $\rm K_D$ (PYR) (*: p < 0.1, **: p < 0.05, ***: p < 0.01).

Bs DHFR Mutant	TMP		PYR	PYR	
	K _D (nM)	K_D (wild type)/ K_D (mutant)	K _D (nM)	K_D (wild type)/ K_D (mutant)	$K_{\rm D~(TMP)}/K_{\rm D}$ (PYR)
Wild Type	8.0 ± 1.3 (n = 4)		12 ± 4 (n = 4)		0.7 ± 0.2
His38Gln	7.8 ± 1.1	1.0	23 ± 4	0.5	0.3 \pm 0.1 *
His38Thr	18 ± 2	0.4	$\begin{array}{c} \textbf{2.8} \pm \\ \textbf{1.2} \end{array}$	4.3	6.5 \pm 3.0 *
His38Val	5.3 ± 1.9	1.5	7 ± 2	1.7	0.8 ± 0.4
Ala39Ile	22 ± 7	0.4	$\begin{array}{c} \textbf{4.8} \pm \\ \textbf{0.6} \end{array}$	2.5	4.5 ± 1.6
Ala39Arg	$17.8 \pm \\1.5$	0.4	6 ± 4	2.0	3.0 ± 1.9
Ala39Tyr	$\begin{array}{c} 14.2 \; \pm \\ 0.9 \end{array}$	0.6	$\begin{array}{c} \textbf{5.5} \pm \\ \textbf{1.7} \end{array}$	2.2	$\begin{array}{c} 2.6 \pm 0.5 \\ *** \end{array}$
Ile40Ala	28 ± 14	0.3	$\begin{array}{c} \textbf{8.4} \pm \\ \textbf{1.8} \end{array}$	1.4	3.3 ± 1.8
Ile40Asn	$120 \pm \\ 30 **$	0.07	18 ± 4	0.7	$6.7 \pm 2.2 \ **$
Ile40Arg	$\begin{array}{c} 150 \; \pm \\ 20 \; ** \end{array}$	0.05	$\begin{array}{c} 23 \; \pm \\ 11 \end{array}$	0.5	6.9 \pm 3.6 **

3.2. TMP and PYR binding and selectivity

To determine the effects of amino acid replacements in the His38-Ala39-Ile40 cluster on inhibitor binding and selectivity, we measured K_D values of the Bs DHFR mutants for the two antifolates, TMP and PYR, by intrinsic protein fluorescence [32,33]. The Bs DHFR has several fluorescently-active aromatic residues (9 Phe, 3 Trp, and 6 Tyr), which allow for tracking of conformational changes by changes in intrinsic protein fluorescence. NADPH cofactor, which is present in the cellular environment, was included in the assays at 100 μ M to determine physiologically relevant K_D values. Whether or not NAPDH is bound can impact inhibitor K_D values; for example, TMP was found to bind L. case DHFR 135 times more tightly when NADPH was also bound compared to when it was not [34]. K_D values were determined at equilibrium by exciting fluorescently-active residues at 290 nm and recording emission intensities of NADPH at 450 nm (resulting from fluorescence energy

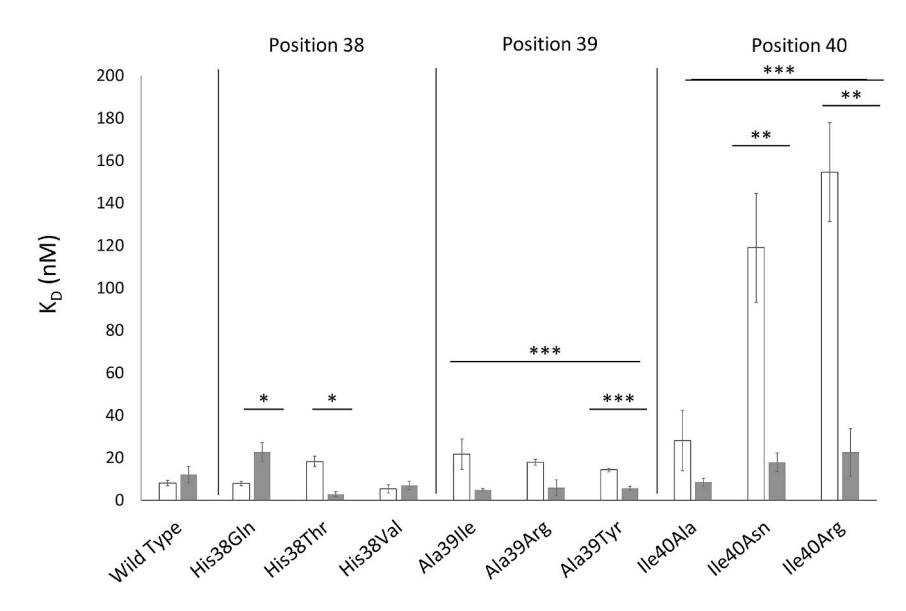


Fig. 3. Bar graph representation of TMP (white bars) and PYR (grey bars) K_D data for Bs DHFR mutants. Error bars represent standard error of at least three replicate measurements. Asterisks indicate significant differences between TMP and PYR K_D values for an individual mutant or residue position. *: p < 0.1, **: p < 0.05, ***: p < 0.01. Bars spanning a residue position indicate a significant difference between TMP and PYR K_D values when considering all the perturbations that were studied at that position.

resonance transfer) in the presence of different concentrations of TMP or PYR. The data was corrected for inner filter effects, as was described previously [2,28,33]. We adapted the intrinsic protein fluorescence protocols to a Synergy H1 microplate reader to improve throughput, compared with the original assay performed in a cuvette. An additional advantage of this approach was that the emission intensity values for each drug concentration were measured simultaneously. This setup allowed longer incubation times (>30 min), assuring that the inhibitor: enzyme:NADPH equilibrium had been reached before measurement [27].

The wild type enzyme binds TMP with a K_D of 8.0 ± 1.3 nM (Table 2). Eight of the nine mutations resulted in reduced TMP affinities (Fig. 3). All three replacements studied at position 40 removed the hydrophobic side chain and resulted in reduced TMP affinities. Statistically significant changes in TMP binding were observed for Ile40Asn and Ile40Arg, which had 15- and 19-fold higher TMP K_D values compared to wild type, respectively (t(2) = 4.33, p < 0.051 and t(2) = 6.26, p = 0.023, Table 2). At position 39, all mutations introduced bulkier side chains and yielded 2 to 3-fold increases in TMP KD, regardless of the side chain introduced. The effects of mutations at position 39 on TMP binding were smaller than those observed at position 40. The orientation of the position 40 side chain towards the active site may explain the greater impact of mutations compared to position 39 on TMP binding. Mutations at position 38 had smaller effects on TMP binding with the introduction of Thr and Val resulting in slightly decreased and increased affinities, respectively.

His38-Ala39-Ile40 cluster mutations in Bs DHFR had different effects on the binding of two competitive DHFR inhibitors, TMP and PYR. All but one mutation resulted in decreased TMP affinities. In contrast, five mutations (His38Thr, His38Val, Ala39Ile, Ala39Arg, and Ala39Tyr) resulted in increased PYR affinities compared with the wild type (12 ± 4 nM). Interestingly, mutants at position 39 had effects of similar magnitude (2-2.5-fold) but in the opposite direction for TMP and PYR. At position 38, two of the mutants (His38Thr and His38Val) resulted in higher PYR affinity, while the His38Gln mutation decreased affinity. The specific sidechain introduced had more impact on inhibitor binding at position 38 than positions 39 and 40. Mutants studied at position 40 had minimal effects on PYR binding: the largest change was a 2-fold decrease in affinity for Ile40Arg. This is in stark contrast to the large decreases observed in TMP binding for position 40 mutants.

As an overall proxy measure for inhibitor selectivity, we calculated the ratio of K_D (TMP) to K_D (PYR) as that mutant's selectivity score. Defined in this way, a ratio greater than 1.0 indicates that the mutant

Table 3

Turnover number ($k_{\rm cat}$) for the wild type, Arg19Asp, and Asp27Asn *Bs* DHFR proteins. Slopes of absorbance at 340 nm with time (s) were converted to velocities using the extinction coefficient 13.2 mM⁻¹cm⁻¹ and a 0.46 cm pathlength [25]. Values represent averages of replicate measurements and are presented with standard errors. The Michaelis constant was determined using the redox sensitive MTS reagent as described in methods section 2.5. *n = 2.

	$k_{\rm cat}$ (s ⁻¹)	K _M (μM)	$k_{ m cat~(wild~type)}/k_{ m cat}$ (mutant)	$K_{\rm M}$ (wild type)/ $K_{\rm M}$ (mutant)
Wild Type	8.1 ± 0.5	$\begin{array}{c} 1.6 \; \pm \\ 0.4 \end{array}$	1	1
Arg19Asp	$\begin{array}{c} 0.072 \; \pm \\ 0.003 \end{array}$	$\begin{array}{c} 17.6 \; \pm \\ 0.7^* \end{array}$	110	0.09
Asp27Asn	$\begin{array}{c} 0.0083 \; \pm \\ 0.0005 \end{array}$	ND	980	ND

binds PYR more tightly than TMP. For the wild type Bs DHFR, the selectivity score is close to 1 (0.7 \pm 0.2, Table 2), suggesting there is little selectivity for either TMP or PYR. Of the nine mutations introduced, five (His38Gln, His38Thr, Ala39Tyr, Ile40Asn, and Ile40Arg) resulted in a significant preference for one ligand over the other (p < 0.1). Perturbations at positions 39 and 40 appeared to result in PYR selective enzymes. Selectivities ranged from 2.6-fold (Ala39Tyr) to 6.9fold (Ile40Arg), three of which had a K_D that was significantly smaller for PYR as compared to TMP (Ala39Tyr: t(2) = 14.151, p = 0.005; Ile40Asn: t(2) = 4.34, p = 0.049; Ile40Arg: t(2) = 5.58, p = 0.031). Mutations at position 38 also influenced selectivity but were dependent on the specific sidechain introduced. Like mutations at other positions, the His38Thr mutation resulted in a large and significant 6.5-fold preference for PYR, a (His38Thr: t(2) = 4.19, p = 0.052). In contrast, the His38Gln mutant was found to bind TMP more tightly than PYR (His38Gln: t(2) = 3.25, p = 0.083), and the His38Val mutant did not impact selectivity. In total, seven out of nine mutations had a ratio >1, reflecting an overall tendency for increased selectivity towards PYR binding upon perturbation to the His38-Ala39-Ile40 cluster. All replacements at positions 39 and 40 resulted in PYR-selective enzymes.

3.3. Steady-state kinetics of Asp27Asn and Arg19Asp Bs DHFR variants

We additionally introduced two mutations into *Bs* DHFR at regions that are catalytically relevant in *Ec* DHFR (*Escherichia coli*), the active site and the Met20 loop. Asp27 is found in the active site of *Ec* DHFR and plays a critical role in the protonation of DHF; the Asp27Asn mutation

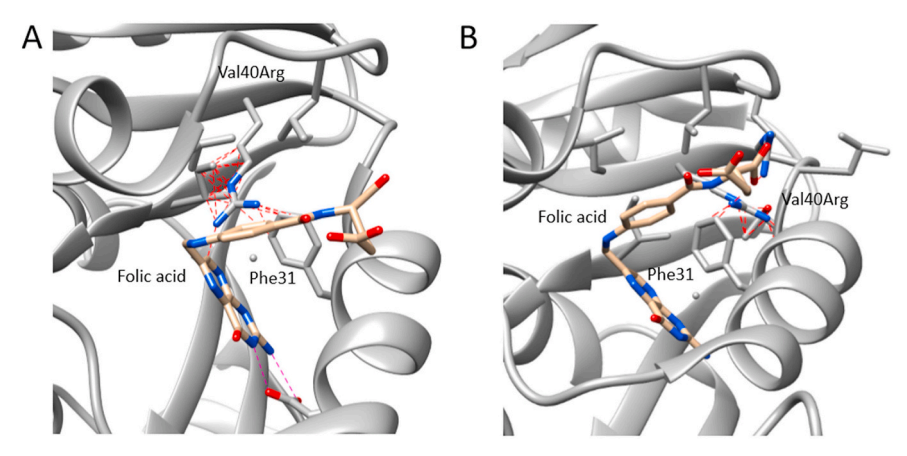


Fig. 4. (A) The Val40Arg mutation was modeled into the Ec DHFR:NADP+:folic acid structure (PDB #: 7DFR) using the Rotamer tool in Chimera (version 1.11.2), choosing the highest probability rotamer determined by the "Dunbrack backbone-dependent rotamer library" (version 1.11.2) [40]. Predicted steric clashes are indicated by red dashed lines as determined using the Find Clashes/Contacts tool, while blue dashed lines indicate hydrogen bonding using the FindHBond tool. (B) The Val40Arg mutation modeled into the Ec DHFR:NADP+: folate structure (PDB #: 7DFR) using the Rotamer tool in Chimera (version 1.11.2) and choosing the second highest probability rotamer [40]. Predicted steric clashes are indicated by red dashed lines determined using the Find Clashes/Contacts tool. (For interpretation of the references to colour in this figure legend, the reader is referred to the Web version of this article.)

resulted in a 300-fold decrease of the hydride transfer step in Ec DHFR [8,35]. Because Asp27 in Ec DHFR aligns with Asp27 in Bs DHFR (Fig. 2), we replaced Asp27 of Bs DHFR with Asn to investigate whether Asp27 also plays a critical role in Bs DHFR catalysis. The k_{cat} for the Asp27Asn mutant was found to be $0.0083 \pm 0.0005 \, \mathrm{s}^{-1}$, a 980-fold reduction compared to the wild type, indicating that Asp27 is a critical active site residue in both Bs and Ec DHFRs (Table 3). Due to the large reduction in activity, we were unable to determine the $K_{\rm M}$ of the Asp27Asn Bs DHFR for comparative analysis.

The Met20 loop is a highly mobile region of bacterial DHFR enzymes and has been reported to be involved in ligand binding and catalysis [36]. The Ec DHFR Met20 loop (residues 9–24) has been extensively studied and critical residues that stabilize the major conformers in catalysis (the open, closed, and occluded conformations) have been identified [1,37]. In E. coli DHFR, the Met20 loop adopts different conformations in response or preparation for NADPH and DHF binding (open), as well as orienting the two molecules for catalysis (closed) and THF release (occluded) [1]. It has been suggested that movement of the Met20 loop is a limiting step in catalysis for bacterial but not mammalian DHFRs, owing to a poly-proline region that locks the mammalian Met20 loop in a closed conformation. Additionally, amino acid replacements in the Ec DHFR have been shown to impact catalysis and loop motions [1,38,39]. To investigate the role of the Met20 loop on Bs DHFR catalysis, we replaced Arg19 in Bs DHFR by Asp. This amino acid replacement results in charge reversal; the negatively charged Asp is conserved among Mycobacterium tuberculosis DHFR (Mt DHFR) and higher organisms at the corresponding alignment position (Fig. 2). The k_{cat} for Arg19Asp was 0.072 ± 0.003 s $^{-1}$, which was 110-fold lower than the $k_{\rm cat}$ of the wild type enzyme (8.1 \pm 0.5 s⁻¹) (Table 3). The K_M for this mutant was 17.6 \pm 0.7 $\mu M,$ 11-fold higher than the wild type K_M of 1.6 \pm 0.4 μ M, indicating that substrate binding also was affected by this mutation.

4. Discussion

4.1. Impact of His38-Ala39-Ile40 cluster mutations on Bs DHFR catalysis

Eight out of the nine mutations of the His38-Ala39-Ile40 cluster had $k_{\rm cat}$ values within 2-fold of the wild type, with non-significant changes in $K_{\rm M}$. This finding suggests that substrate binding was not drastically affected by introducing these mutations and any inhibitor preferences arising from these mutations are not due to inactivation of the enzyme. Only the Ile40Arg mutant showed significant changes in both $k_{\rm cat}$ and $K_{\rm M}$. To better understand the increased $K_{\rm M}$ for the Ile40Arg mutant, we used the Ec DHFR:NADP+:folate structure (PDB #: 7DFR) as a model. We used the Rotamers function in Chimera to replace the residue that aligned with Ile40 in Bs DHFR — a valine at position 40 in Ec DHFR — with an Arg in silico (Chimera version 1.11.2) (Fig. 4) [30,40]. The two

most probable predicted rotamers of Arg40 in the "in silico-Val40Arg mutant" sterically clashed with nearby moieties, including Phe31 and folic acid. These clashes may possibly explain the observed increase in K_M for Bs DHFR Val40Arg when compared to wild type [30,40]. Mutagenesis studies of Hs DHFR at the Phe34 residue (Phe31 in Bs DHFR) have implicated it as a ligand-selectivity determinant, as it forms important contacts with methotrexate and DHF [32]. Therefore, a mutation that results (by domino effect) in an altered position of Phe31 (Bs DHFR numbering) may contribute to the observed decrease in substrate affinity. The relatively small changes in k_{cat} and K_{M} (Table 1) suggest that the cluster mutations did not result in large scale deviations in structure. Moreover, the CD spectra for the wild type, Ile40Asn, and Ile40Arg Bs DHFRs shown in Supplement Fig. S2 are similar to each other and in agreement with previously published spectra for DHFR [41], implying that mutations at Ile40 did not cause any secondary structural changes as compared to the wild type Bs DHFR structure.

4.2. Impacts of His38-Ala39-Ile40 cluster mutations on TMP and PYR binding and selectivity

Our results suggest that the His38-Ala39-Ile40 cluster is a distal determinant for inhibitor selectivity as was previously predicted in the DHFR family [16]. The residue sidechains of the cluster do not make direct contact with the inhibitors themselves; yet mutating these residues results in selectivity toward one inhibitor over another. The literature has reported on long-distance effects from distal sites in DHFR catalysis, substrate binding, and product release [1]. Changes to relative energies and, subsequently, the conformational equilibria, where the enzyme samples multiple conformations that bind ligands with different affinities, can perhaps explain these results [18,19]. It is interesting that the perturbations at this cluster resulted in preference for PYR binding over TMP, even though both inhibitors occupy the same region of the active site [42]. A major difference between the two inhibitors is a one carbon linker in TMP, which adds more degrees of rotational freedom compared to PYR. It is possible that the mutations affected TMP binding more due to the compound's greater flexibility [43,44].

The *Mt* DHFR has been crystallized as a ternary complex with NADPH and both TMP (PDB#: 4KM2) and PYR (PDB#: 4KM0) in two conformations (open and closed), making these structures useful in understanding of the interactions between DHFR:NADPH and the two inhibitors [43,44]. By solving the X-ray crystal structures, Dias et al. found that TMP binding differs between the open and closed conformations and that this difference is greater than what is observed with PYR [43,44]. Between the two conformations, the trimethoxybenzyl ring of TMP orients itself toward or away from the active site, causing interacting sidechains Phe31, Leu50, and Ile120 to reorganize [43,44]. A greater reliance on sidechain reorganization may make TMP binding more susceptible to perturbations resulting from mutations of a distant

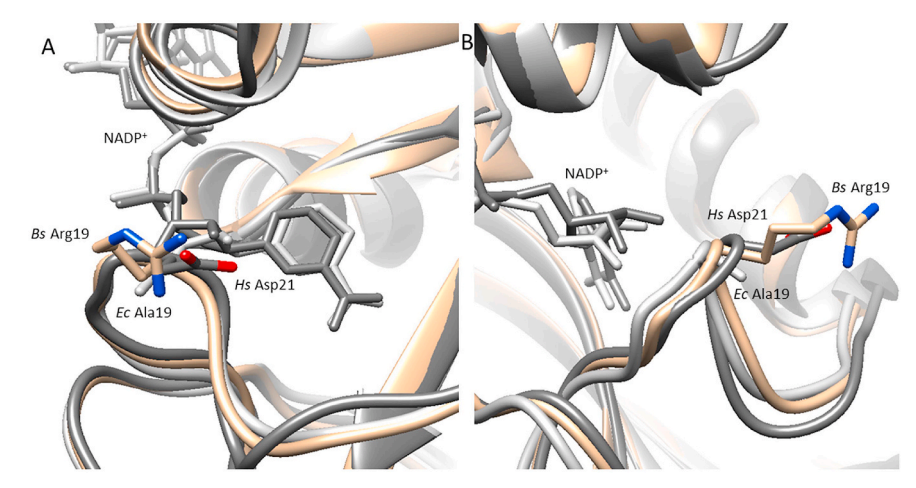


Fig. 5. Cartoon representation of the *Bs* DHFR (tan, PDB #: 1ZDR), *Hs* DHFR (dark grey, PDB #: 2W3A) and the *Ec* DHFR with the Met20 loop the closed (light grey, PDB #: 1RH3) conformation. (A) Labels accompany aligned residues with their native numbering. NADP⁺ is shown and labeled in both the *Hs* (dark grey) and *Ec* (light grey) structures. (B) Another view that shows all residues pointing towards the solvent in crystal structures. Both panels were made in Chimera (version 1.11.2) using the Match Maker tool [30].

amino acid [19,20,45]. This may explain why mutations of the His38-Ala39-Ile40 cluster tended to decrease TMP affinity, causing PYR binding to be preferred.

4.3. Asp27 and Arg19 play similar roles as the equivalent residues in Ec DHFR

The reduced activity of Asp27Asn was not surprising as all DHFRs show conservation of a negatively charged residue at this alignment position (Fig. 2) [1]. Findings by Wan et al. suggest that a negative charge aids catalysis by increasing the pK_a of the active site, allowing easier protonation of the N5 atom of the pterin ring by a water molecule [46]. The significant decrease in activity observed for the Bs DHFR Asp27Asn mutation agrees with the mechanism for Ec DHFR catalysis presented by Wan and coauthors. CD spectroscopy also showed a change in secondary structure for Asp27Asn compared to the wild-type protein (Fig. S3), which could also contribute to the decreased catalytic activity. We do not report percentages of different secondary structure elements in the Bs DHFR proteins because analyzing these by CD has been reported to be complicated by the numerous aromatic residues in DHFR sequences [41].

The Bs DHFR (PDB#: 1ZDR) Arg19 residue spatially overlaps with the Asp21 residue in Hs DHFR (PDB#: 2W3A) and the Ala19 residue of Ec DHFR (PDB#: 1RH3) (Fig. 5). In the aligned structures, the residue at this alignment position points out toward the solvent, and does not show any sidechain interactions with NADP⁺ in the Ec and Hs structures (Fig. 5). Therefore, we find it unlikely that the reduced activity for the Arg19Asp mutant is caused by altered noncovalent interactions.

5. Conclusions

In summary, experimental data support the prediction that the His38-Ala39-Ile40 cluster is a distal region that tunes inhibitor selectivity. Analysis of Bs DHFR mutants at His38, Ala39, and Ile40 indicates that these replacements can lead to small changes in k_{cat} and K_{M} while significantly affecting inhibitor affinity and selectivity. We found all mutations at cluster positions 39 and 40 to increase selectivity for PYR binding over TMP; that is, the variants had higher affinities for PYR than TMP. Mutations at this cluster may have affected inhibitor selectivity by perturbing the preorganization process, where the enzyme samples multiple conformations in preparation for inhibitor binding and catalysis. It is unlikely that a distal region such as the His38-Ala39-Ile40 cluster uniquely impacts inhibitor selectivity in the DHFR superfamily. In fact, the same in silico study predicted two additional regions to affect inhibitor selectivity. Further studies are being conducted to elucidate their effects on inhibitor selectivity and to further verify the in silico model. A better understanding of distal regions that dictate ligand

selectivity will be valuable for *in silico* modeling, protein engineering, and the drug discovery process.

Acknowledgements

We are grateful to the National Institutes of Health (#1R15GM126467-01), the National Science Foundation S-STEM grant (DUE-1458499), the Novartis Scholarship, and the Science Honors Innovation Program (SHIP) for supporting student researchers and the Montclair State University Separately Budgeted Research Award for other funding. We thank Sarah Hall, Emily Egbert, Maureen Malivert, and Dina Edani for technical assistance. We thank Tamara Kreiss and Keith Lange for helpful discussions. We thank Adam Parker and the Montclair State Biology Department for sequencing the mutant plasmids for this project.

Appendix A. Supplementary data

Supplementary data to this article can be found online at https://doi.org/10.1016/j.abb.2020.108545.

References

- J.R. Schnell, H.J. Dyson, P.E. Wright, Structure, dynamics, and catalytic function of dihydrofolate reductase, Annu. Rev. Biophys. Biomol. Struct. 33 (1) (2004) 119–140.
- [2] J.R. Appleman, E.E. Howell, J. Kraut, M. Kühl, R.L. Blakley, Role of aspartate 27 in the binding of methotrexate to dihydrofolate reductase from *Escherichia coli*, J. Biol. Chem. 263 (19) (1988) 9187–9198.
- [3] G.M. Eliopoulos, P. Huovinen, Resistance to trimethoprim-sulfamethoxazole, Clin. Infect. Dis. 32 (11) (2001) 1608–1614.
- [4] A.C. Anderson, Targeting DHFR in parasitic protozoa, Drug Discov. Today 10 (2) (2005) 121–128.
- [5] P. Kongsaeree, P. Khongsuk, U. Leartsakulpanich, P. Chitnumsub, B. Tarnchompoo, M.D. Walkinshaw, Y. Yuthavong, Crystal structure of dihydrofolate reductase from *Plasmodium vivax*: pyrimethamine displacement linked with mutation-induced resistance, Proc. Natl. Acad. Sci. U.S.A. 102 (37) (2005) 13046–13051.
- [6] O. Sköld, A. Widh, A new dihydrofolate reductase with low trimethoprim sensitivity induced by an R factor mediating high resistance to trimethoprim, J. Biol. Chem. 249 (13) (1974) 4324–4325.
- [7] S.F. Chowdhury, V.B. Villamor, R.H. Guerrero, I. Leal, R. Brun, S.L. Croft, J. M. Goodman, L. Maes, L.M. Ruiz-Perez, D.G. Pacanowska, Design, synthesis, and evaluation of inhibitors of trypanosomal and leishmanial dihydrofolate reductase, J. Med. Chem. 42 (21) (1999) 4300–4312.
- [8] E.E Howell, J.E. Villafranca, M.S. Warren, S.J. Oatley, J. Kraut, Functional role of aspartic acid-27 in dihydrofolate reductase revealed by mutagenesis, Science 231 (1986) 1123–1128.
- [9] K.M. Perry, J.J. Onuffer, N.A. Touchette, C.S. Herndon, M.S. Gittelman, R. C. Matthews, J.T. Chen, R.J. Mayer, K. Taira, Effect of single amino acid replacements on the folding and stability of dihydrofolate reductase from *Escherichia coli*. Biochemistry 26 (10) (1987) 2674–2682.
- [10] M. Watson, J.W. Liu, D. Ollis, Directed evolution of trimethoprim resistance in Escherichia coli, FEBS J. (274) (2007) 2661–2671.

- [11] C.T. Liu, F. Kevin, P.L. Joshua, H. Xinyi, H.-S. Sharon, K. Amnon, J.B. Stephen, Escherichia coli dihydrofolate reductase catalyzed proton and hydride transfers: temporal order and the roles of Asp27 and Tyr100, Proc. Natl. Acad. Sci. U.S.A. 111 (51) (2014) 18231–18236.
- [12] A.R. Mhashal, A. Vardi-Kilshtain, A. Kohen, D.T. Major, The role of the Met20 loop in the hydride transfer in *Escherichia coli* dihydrofolate reductase, J. Biol. Chem. 292 (34) (2017) 14229–14239.
- [13] H. Abdizadeh, Y.T. Tamer, O. Acar, E. Toprak, A.R. Atilgan, C. Atilgan, Increased substrate affinity in the *Escherichia coli* L28R dihydrofolate reductase mutant causes trimethoprim resistance, Phys. Chem. Chem. Phys. 19 (18) (2017) 11416–11428.
- [14] D.A. Ragland, E.A. Nalivaika, M.N.L. Nalam, K.L. Prachanronarong, H. Cao, R. M. Bandaranayake, Y. Cai, N. Kurt-Yilmaz, C.A. Schiffer, Drug resistance conferred by mutations outside the active site through alterations in the dynamic and structural ensemble of HIV-1 protease, J. Am. Chem. Soc. 136 (34) (2014) 11956–11963.
- [15] P.K. Agarwal, N. Doucet, C. Chennubhotla, A. Ramanathan, C. Narayanan, Conformational sub-states and populations in enzyme catalysis, Methods Enzymol. 578 (2016) 273–297.
- [16] N.M. Goodey, K.G. Herbert, S.M. Hall, K.C. Bagley, Prediction of residues involved in inhibitor specificity in the dihydrofolate reductase family, Biochim. Biophys. Acta 1814 (12) (2011) 1870–1879.
- [17] A.N. Naganathan, Modulation of allosteric coupling by mutations: from protein dynamics and packing to altered native ensembles and function, Curr. Opin. Struct. Biol. 54 (2019) 1–9.
- [18] J.F. Swain, L.M. Gierasch, The changing landscape of protein allostery, Curr. Opin. Struct. Biol. 16 (1) (2006) 102–108.
- [19] N.M. Goodey, S.J. Benkovic, Allosteric regulation and catalysis emerge via a common route, Nat. Chem. Biol. 4 (8) (2008) 474–482.
- [20] M.-H. Seo, J. Park, E. Kim, S. Hohng, H.-S. Kim, Protein conformational dynamics dictate the binding affinity for a ligand, Nat. Commun. 5 (2014) 3724.
- [21] N.M. Goodey, M.T. Alapa, D.F. Hagmann, S.G. Korunow, A.K. Mauro, K.S. Kwon, S. M. Hall, Development of a fluorescently labeled thermostable DHFR for studying conformational changes associated with inhibitor binding, Biochem. Biophys. Res. Commun. 413 (3) (2011) 442–447.
- [22] H.S. Kim, S.M. Damo, S.-Y. Lee, D. Wemmer, J.P. Klinman, Structure and hydride transfer mechanism of a moderate thermophilic dihydrofolate reductase from *Bacillus stearothermophilus* and comparison to its mesophilic and hyperthermophilic homologues, Biochemistry 44 (34) (2005) 11428–14439.
- [23] J. Barbet, S. Huclier-Markai, Equilibrium, affinity, dissociation constants, IC5O: facts and fantasies, Pharmaceut. Stat. (2019), 0(0).
- [24] L. Zheng, U. Baumann, J.-L. Reymond, An efficient one-step-directed and sitesaturation mutagenesis protocol, Nucleic Acids Res. 32 (14) (2004) e115.
- [25] A.M. Tobias, D. Toska, K. Lange, T. Eck, R. Bhat, C.A. Janson, D.P. Rotella, U. Gubler, N.M. Goodey, Expression, purification, and inhibition profile of dihydrofolate reductase from the filarial nematode *Wuchereria bancrofti*, PloS One 13 (5) (2018), e0197173.
- [26] C.R. Bourne, E.W. Barrow, R.A. Bunce, P.C. Bourne, K.D. Berlin, W.W. Barrow, Inhibition of antibiotic-resistant *Staphylococcus aureus* by the broad-spectrum dihydrofolate reductase inhibitor RAB1, Antimicrob. Agents Chemother. 54 (9) (2010) 3825–3833.
- [27] E.C. Hulme, M.A. Trevethick, Ligand binding assays at equilibrium: validation and interpretation, Br. J. Pharmacol. 161 (6) (2010) 1219–1237.
- [28] B. Birdsall, R.W. King, M.R. Wheeler, C.A.J. Lewis, S.R. Goode, R.B. Dunlap, G.C. K. Roberts, Correction for light absorption in fluorescence studies of Protein-Ligand Interactions, Anal. Biochem. (1983) 353–361.
- [29] J.F. Morrison, Kinetics of the reversible inhibition of enzyme-catalysed reactions by tight-binding inhibitors, Biochim. Biophys. Acta 185 (2) (1969) 269–286.

- [30] E.F. Pettersen, T.D. Goddard, C.C. Huang, G.S. Couch, D.M. Greenblatt, E.C. Meng, T.E. Ferrin, UCSF Chimera—a visualization system for exploratory research and analysis, J. Comput. Chem. 25 (13) (2004) 1605–1612.
- [31] Landmark Database Blast, National Library of Medicine (US), National Center for Biotechnology Information: National Center for Biotechnology Information, Bethesda (MD, 2004 (NCBI); [accessed Mar. 10 2020], https://www.ncbi.nlm.nih.gov/
- [32] J.P. Volpato, E. Fossati, J.N. Pelletier, Increasing methotrexate resistance by combination of active-site mutations in human dihydrofolate reductase, J. Mol. Biol. 373 (3) (2007) 599–611.
- [33] R. Perez-Abraham, K.G. Sanchez, M. Alfonso, U. Gubler, J.J. Siekierka, N. M. Goodey, Expression, purification and enzymatic characterization of *Brugia malayi* dihydrofolate reductase, Protein Expr. Purif. 128 (2016) 81–85.
- [34] J. Feeney, B. Birdsall, N.V. Kovalevskaya, Y.D. Smurnyy, E.M. Navarro Peran, V. I. Polshakov, NMR structures of apo L. casei dihydrofolate reductase and its complexes with trimethoprim and NADPH: contributions to positive cooperative binding from ligand-induced refolding, conformational changes, and interligand hydrophobic interactions, Biochemistry 50 (18) (2011) 3609–3620.
- [35] P. Shrimpton, R.K. Allemann, Role of water in the catalytic cycle of E. coli dihydrofolate reductase, Protein Sci. 11 (6) (2002) 1442–1451.
- [36] L.Y.P. Luk, J.J. Ruiz-Pernía, W.M. Dawson, E.J. Loveridge, I. Tuñón, V. Moliner, R. K. Allemann, Protein isotope effects in dihydrofolate reductase from *Geobacillus stearothermophilus* show entropic–enthalpic compensatory effects on the rate constant, J. Am. Chem. Soc. 136 (49) (2014) 17317–17323.
- [37] D. McElheny, J.R. Schnell, J.C. Lansing, H.J. Dyson, P.E. Wright, Defining the role of active-site loop fluctuations in dihydrofolate reductase catalysis, Proc. Natl. Acad. Sci. U.S.A. 102 (14) (2005) 5032–5037.
- [38] C.T. Liu, P. Hanoian, J.B. French, T.H. Pringle, S. Hammes-Schiffer, S.J. Benkovic, Functional significance of evolving protein sequence in dihydrofolate reductase from bacteria to humans, Proc. Natl. Acad. Sci. U.S.A. 110 (25) (2013) 10159–10164.
- [39] G. Bhabha, D.C. Ekiert, M. Jennewein, C.M. Zmasek, L.M. Tuttle, G. Kroon, H. J. Dyson, A. Godzik, I.A. Wilson, P.E. Wright, Divergent evolution of protein conformational dynamics in dihydrofolate reductase, Nat. Struct. Mol. Biol. 20 (11) (2013) 1243–1249.
- [40] R.L. Dunbrack Jr., Rotamer libraries in the 21st century, Curr. Opin. Struct. Biol. 12 (4) (2002) 431–440.
- [41] E. Ohmae, S. Tanaka, Y. Miyashita, K. Katayanagi, K. Matsuo, Vacuum-ultraviolet circular dichroism spectra of Escherichia coli dihydrofolate reductase and its mutants: contributions of phenylalanine and tyrosine side chains and exciton coupling of two tryptophan side chains, J. Phys. Chem. B (2015) 1520–5207 (Electronic).
- [42] J. Feeney, NMR studies of ligand binding to dihydrofolate reductase, Angew. Chem. Int. Ed. 39 (2) (2000) 290–312.
- [43] M.V. Dias, P. Tyrakis, R.R. Domingues, A.F. Paes Leme, T.L. Blundell, Mycobacterium tuberculosis dihydrofolate reductase reveals two conformational states and a possible low affinity mechanism to antifolate drugs, Structure 22 (1878–4186) (2014) 94–103 (Electronic).
- [44] J.A. Ribeiro, S.A.-O. Chavez-Pacheco, G.S. de Oliveira, C.D.S. Silva, J.H.P. Giudice, G.A. Libreros-Zuniga, M.V.B. Dias, Crystal structures of the closed form of *Mycobacterium tuberculosis* dihydrofolate reductase in complex with dihydrofolate and antifolates, Acta Crystallogr. D Struct. Biol. D75 (2059-7983) (2019) 682–693 (Electronic).
- [45] D.D. Boehr, J.R. Schnell, D. McElheny, S.-H. Bae, B.M. Duggan, S.J. Benkovic, H. J. Dyson, P.E. Wright, A distal mutation perturbs dynamic amino acid networks in dihydrofolate reductase, Biochemistry 52 (27) (2013) 4605–4619.
- [46] Q. Wan, B.C. Bennett, M.A. Wilson, A. Kovalevsky, P. Langan, E.E. Howell, C. Dealwis, Toward resolving the catalytic mechanism of dihydrofolate reductase using neutron and ultrahigh-resolution X-ray crystallography, Proc. Natl. Acad. Sci. U.S.A. 111 (2014) 18225–18230.